KR INCORPORATION IN SPUTTERED AMORPHOUS SI LAYERS

Greuter, M. J. W.; Niesen, L.; van Veen, A.; Hakvoort, R. A.; Verwerft, M.; de Hosson, J. Th. M.; Berntsen, A. J. M.; Sloof, W. G.

Published in:
Journal of Applied Physics

DOI:
10.1063/1.358641

Publication date:
1995

Kr incorporation in sputtered amorphous Si layers

M. J. W. Greuter[a] and L. Niesen
Nuclear Solid State Physics, Materials Science Centre, Groningen University, Nijenborgh 4, 9747 AG Groningen, The Netherlands

A. van Veen and R. A. Hakvoort
Interfaculty Reactor Institute, Delft University of Technology, Mekelweg 15, 2629 JB Delft, The Netherlands

M. Verwerft and J. Th. M. de Hosson
Applied Physics, Materials Science Centre, Groningen University, Nijenborgh 4, 9747 AG Groningen, The Netherlands

A. J. M. Berntsen
Department of Atomic and Interface Physics, Debye Institute, Utrecht University of Technology, P.O. Box 80000, 3508 TA Utrecht, The Netherlands

W. G. Sloof
Laboratory of Materials Science, Delft University of Technology, Rotterdamseweg 137, 2628 AL Delft, The Netherlands

(Received 15 November 1993; accepted for publication 21 December 1994)

Amorphous Si layers were grown by krypton plasma sputter deposition at 310 °C. By pulsation of the substrate potential between 0 and 50 eV, the Kr concentration in the layers could be varied to a maximum of 5.5 at. %. A model which describes trapping of inert gas atoms in the sputtered layer in terms of implantation and trapping, diffusion, growth, resputtering, and gas sputtering is presented. High-resolution electron microscopy, electrode-probe (x-ray) microanalysis, positron annihilation, Raman spectroscopy, Mössbauer spectroscopy, and bending and hardness measurements were performed on the deposited layers. It turns out that the ion assisted growth leads to a strong reduction of open volume defects. The experiments point to the presence of very small Kr agglomerates. From the Mössbauer experiments a lower limit of 250 K for the Debye temperature of the Kr agglomerates is derived. Molecular-dynamic simulations from which the Debye temperatures of Kr mono-, di-, and trimers in amorphous Si can be derived are presented. The simulations indicate the presence of predominantly Kr monomers and dimers. © *1995 American Institute of Physics.*

I. INTRODUCTION

Since the first publication by Barnes in 1960 (Ref. 1) on He in metals, research has shown an increasing interest in the properties of inert gases in materials for fission and fusion reactors. Initially fission gas bubble swelling and gas release from reactor fuels, but later on also the more fundamental aspects of inert gas behavior were under investigation, e.g., inert gas atom diffusion, bubble nucleation, irradiation induced bubble resolution, bubble movement, and pathways for inert gas release. In 1984 an impetus was given to the research on inert gas behavior in materials by the discovery[2,3] that the implantation of heavy inert gas ions (Ar, Kr, and Xe) in metals leads to the formation of room-temperature solid inert gas precipitates. Transmission electron microscopy experiments have shown that the precipitates were epitaxial with the host matrix in most cases. Whereas the majority of these studies have been carried out on inert gas precipitation in metals (for a recent overview on this subject, we refer to Ref. 4), only a few studies have been published on inert gas precipitation in ceramics,[5] alloys,[3,6] and semiconductors.[7,8] The KrAl system has been studied extensively by us[9–11] using Mössbauer spectroscopy on the 9.4 keV transition in ^{83}Kr. Mössbauer spectroscopy on Kr bubbles is a very powerful technique, especially when used in conjunction with electron microscopy analysis, because it provides detailed information on the local environment of the inert gas atoms. Different environments of the ^{83}Kr Mössbauer probe give rise to clearly different components of the spectrum. In particular, the contribution of bulk and interface bubble atoms can be separated. From the relative intensities the size of the bubbles can be inferred. The lattice dynamics can be studied directly by monitoring the recoilless fraction as a function of temperature, from which the Debye temperature can be derived. This quantity and the isomer shift are directly related to the atomic density in the bubbles.

In this paper we discuss the KrSi system. Inert gas ions are used extensively in techniques like ion milling, sputter cleaning, and ion-beam assisted deposition of epitaxial layers. However, very little is known about the final location of these atoms, both in amorphous and in crystalline Si. Plasma sputtering is a relatively simple technique for achieving ion-beam assisted deposition, which enables one to study the different aspects playing a role. Using this technique with a negative bias at the substrate, a considerable flux can be established of low-energy inert gas ions hitting the growing film. Therefore it is easy to prepare deposited films under controlled conditions, with a homogeneous density of incorporated inert gas atoms. In this paper we present model calculations on the incorporation of Kr atoms in sputtered Si

[a]E-mail: H.Hasper@phys.rug.nl

 0021-8979/95/77(7)/3467/12/$6.00

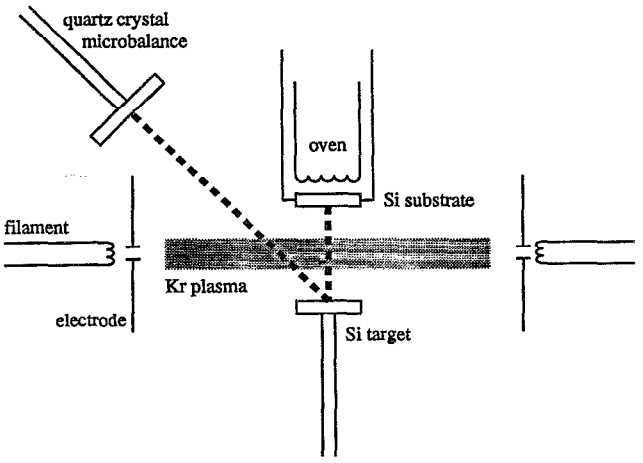

FIG. 1. Schematic drawing of the plasma sputter deposition apparatus.

films. In addition, we will present a microscopic characterization of these films with a variety of experimental techniques.

II. EXPERIMENTAL SETUP

Samples were made with a high-dose desorption spectrometer at the Interfaculty Reactor Institute in Delft. In this apparatus it is possible to ionize and implant gases at energies up to 3 keV and to deposit layers on a substrate.[12] The temperature of the substrate can be controlled from room temperature up to 630 °C, and the ion and atom fluxes at the substrate can be independently controlled by applying a pulsating voltage to the substrate or to the sputter target.

In Fig. 1 a schematic drawing is shown of the plasma sputter deposition apparatus. From the W filaments electrons are emitted which are accelerated by the electrodes at energies which can be varied from 100 to 300 eV. An external magnetic field of ≈0.65 kG parallel to the axis of the two filaments is used to keep the electrons in a helical motion near the axis. Upon approaching the opposite filament, the electrons will be decelerated to zero energy and be reflected. Therefore the electrons will travel back and forth a few times and ionize the inert gas that has been introduced at a pressure of 0.01–0.1 Pa. The result is a ribbon-shaped low-pressure plasma. The plasma has the property that the electron conductivity is high in the axial direction but not in the transversal direction. Therefore, when a transversal electrical field is applied, e.g., for extracting ions toward the target or the substrate, the plasma ribbon will stay in position. Consequently, a distance of about 4 mm suffices to accommodate a potential drop of 1.5 kV. In the apparatus high fluxes of sputtered target atoms and high fluxes of incorporating gas ions can be established, typically 10^{16} cm^{-2} s^{-1}. The sputtered neutral target atoms have energies distributed according to an E^{-2} distribution, with an average energy equal to the average binding energy which equals the cohesion energy of the target material. The angular distribution is a cosine distribution.[13] The amount of sputtered material can be monitored by a quartz-crystal microbalance. Growth rates are of the order of 1 nm s^{-1}. For a detailed description of the apparatus, we refer to Refs. 12 and 14.

TABLE I. Summary of sputtered Kr*Si* layers.

Sample No.	J_{Kr}/J_{Si}	Duty cycle (%)	Frequency (Hz)	Kr conc. (at. %)
1	0.10	1	10	0.38
2	0.15	2	10	0.49
3	0.41	5	10	1.0
4	1.2	10	0.5	2.6
5	2.8	20	0.5	3.7
6	2.9	30	0.5	4.7
7	4.9	50	0.5	5.6
8	12.6	100	0.5	3.0
9	21.0	200	0.5	2.6

III. EXPERIMENTAL PROCEDURE

Thin films were produced by sputtering of Si in a low-pressure (0.01–0.1 Pa) Kr plasma as described before. In order to incorporate inert gas ions in the growing film, the substrate is at a negative bias with respect to the plasma. The thickness of the sputtered layer was monitored with a quartz-crystal microbalance and calibrated by weighing the deposited film. For our experiments, amorphous Kr*Si* (*a*-Si) films with a diameter of 10 mm were deposited on a Si⟨100⟩ wafer at a temperature of 583 K and a substrate bias of −50 V, using a Si target at a potential of −1.5 kV with respect to the plasma. By varying the duty cycle of the pulsation of the substrate potential between 1% and 100% with a period of 0.1 s for the 1% to 5% and 2 s for the larger duty cycles, the Kr flux J_{Kr} could be varied between 4.4×10^{14} and 4.4×10^{16} cm^{-2} s^{-1}. The Si flux J_{Si} at the substrate was on the average 4×10^{15} cm^2 s^{-1}. In this way several films were deposited with an average thickness of 6 μm. For an overview of the samples produced, see Table I.

Several techniques were used for *ex situ* composition analysis. The Kr concentration in the sputtered Si layers was determined by electron-probe (x-ray) microanalysis (EPMA), employing wavelength dispersive spectrometry (WDS) in plane and in cross-section geometry. Rutherford backscattering (RBS) employing 1 MeV He^+ was used for calibration of the Kr concentration in the top 0.2 μm. The microstructure of the layers has been analyzed by high-resolution electron microscopy (HREM) on cross-sectional samples. Positron beam analysis (PA) was used to characterize defects in the deposited films, in particular the open volume defects.[15,16] Raman spectroscopy is sensitive to structural changes[17] and has been used to probe the bond-angle distortion. Mössbauer spectroscopy has been applied to probe the local environment of the incorporated Kr atoms.[11,18] The deposited layers bent considerably under the strain caused by the high concentration of inert gas atoms. The curvature of the samples has been measured using a conventional light microscope. Finally, we measured the microhardness of the deposited films.

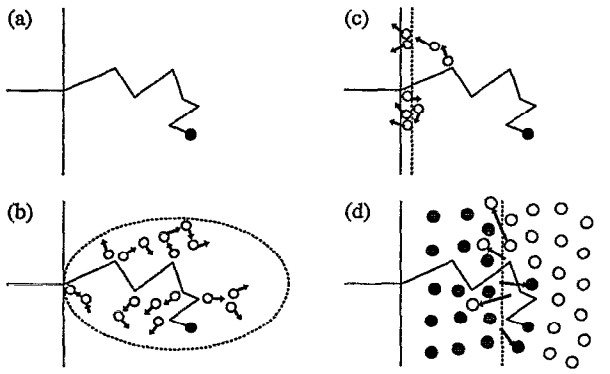

FIG. 2. Interaction processes of low-energy ions with a growing film: (a) ion implantation, (b) collision cascade, (c) surface sputtering, and (d) ion induced mixing.

IV. MODEL FOR ION ASSISTED DEPOSITION

The different processes which play a role in the interaction of low-energy ion beams with a substrate are shown in Fig. 2. The incident ion with energy E_i will interact with the substrate and will finally come to rest at some depth below the surface (a). The ion incorporation will lead to the creation of vacancy/interstitial pairs by direct collisions, usually called the collision cascade (b). The further evolution of the collision cascade can lead to the emission or sputtering of surface atoms of the host material (c). In addition, ion-beam induced mixing (d) will occur. When a sharp interface is present between the substrate and some deposited material, the interface will broaden under the influence of irradiation induced collision cascades. Applied to inert gas implantation, ion-beam mixing will lead to the effect known as gas sputtering,[19,20] since a previously implanted and trapped inert gas atom can reach the surface by collision cascades or by detrapping due to defect mechanisms.

In Fig. 3 a schematic drawing is shown of the relevant ion fluxes in a plasma sputter deposition process. The flux J_0 of Kr^+ ions from the plasma toward the sputter target will lead to sputtering of Si neutrals, represented by J_{Si}. This flux will cause the Si substrate to grow at a velocity v_s. When a negative potential with respect to the plasma is applied to substrate, this will cause a flux J_{Kr} of Kr^+ ions from the plasma to the substrate. The implantation profile of the inert gas atoms in the substrate can be approximated by a Gaussian distribution. So the trapping probability $p(x)$ at depth x beneath the surface can be written as

$$p(x)=p_0\eta e^{-1/2[(x-R_p)/\Delta R_p]^2}, \tag{1}$$

where η is the penetration probability of the Kr ion, p_0 a normalization constant so that $\int p(x)dx=\eta$, R_p the projected range, and ΔR_p the straggling of the implantation profile. The steady-state inert gas concentration $c(x,t)$ of the inert gas atoms at depth x and time t can be written as[16,18]

$$0=\frac{\partial c(x,t)}{\partial t}=J_{Kr}\,p(x)+D\,\frac{\partial^2 c(x,t)}{\partial x^2}+v_s\,\frac{\partial c(x,t)}{\partial x}$$
$$-J_{Kr}\sigma_g(x)c(x,t), \tag{2}$$

where the first term describes the incorporation of inert gas atoms in the growing film by implantation and trapping, Eq. (1), the second term describes the thermal diffusion of the Kr atoms in the sputtered layer, with D the thermal diffusivity, the third term describes the film growth in terms of the surface velocity v_s, and the fourth term describes the gas sputtering in terms of the gas sputtering cross section σ_g. The surface velocity v_s is determined by the deposition and sputtering rate and can be written as

$$v_s=\frac{J_{Kr}Y_{Si}-J_{Si}}{N_0}, \tag{3}$$

where Y_{Si} is the sputtering yield of Si by Kr and N_0 the density of the deposited material. In a simple model of the gas sputtering, the gas sputtering cross section is given by

$$\sigma_g(x)=\sigma_0 e^{-x/\lambda_g}, \tag{4}$$

where σ_0 is the cross section for release of the Kr out of the sputtered layer at very shallow depth and λ_g the effective escape depth of individual Kr atoms in the sputtered layer.

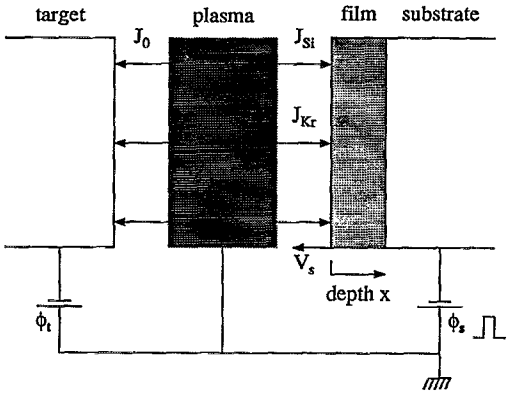

FIG. 3. Schematic drawing of relevant fluxes in the plasma sputter deposition process.

V. EXPERIMENTAL RESULTS

A. Concentration of Kr in deposited Si films as a function of Kr to Si flux ratio

EPMA was employed for quantitative assessment of the concentration of Kr in the sputtered Si films. A JEOL JXA 733 electron-probe x-ray microanalyzer equipped with four wavelength dispersive spectrometers and one energy dispersive system was used. A focused 10 keV electron beam at a current of 100 nA was used for the generation of the characteristic x rays. The intensities of both Si K_α (1.740 keV) and Kr L_α (1.587 keV) were measured simultaneously with wavelength dispersive spectrometers. These intensities were compared with the corresponding intensities of pure Si and a Kr*Si* standard. This standard consisted of a 5 μm thick sputtered Si layer with a uniform Kr concentration of 5.8 at. %, as measured by RBS using 1 MeV He^+. The concentration of

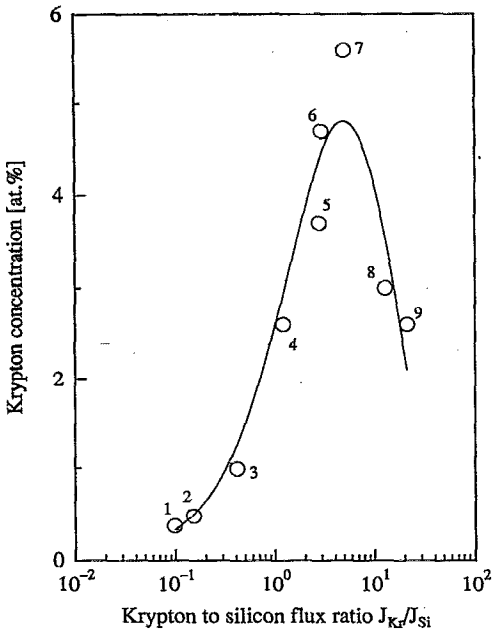

FIG. 4. Concentration of Kr incorporated in sputtered Si films (see Table I) vs the Kr to Si flux ratio as measured by WDS. The full line is a model calculation, Eq. (2), with the parameters listed in Table II.

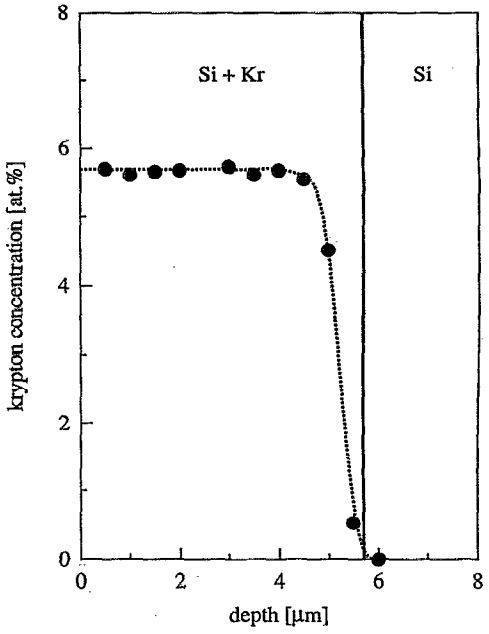

FIG. 5. Cross-sectional EDS results of Kr concentration (●) vs depth. The dotted curve serves to guide the eye. The layer to bulk interface is indicated by a vertical bar. The low Kr concentration in the first 1 μm in the layer is caused by tilting the sample during the EDS measurement. The errors are ± 0.5 μm.

Kr in the sputtered films was determined from the intensity ratios applying the modified $\Phi(\rho z)$ approach for matrix corrections.[21]

The Kr concentration of the sputtered a-Si layers as a function of the Kr to Si flux ratio J_{Kr}/J_{Si} as measured by EPMA is shown in Fig. 4. A maximum concentration of $\approx$5.5 at. % is reached for $J_{Kr}/J_{Si}=5$. The experimental points are fitted to the incorporation model given by Eq. (2); the fit is shown in Fig. 4 by the solid line. As can be seen from the figure, the correspondence between the experiment and the model as described in the previous section is satisfactory. The corresponding fitted parameters are listed in Table II and are compared with the experimental values obtained for c-Si.[16] The trapping factor p_0 is a factor of 10 smaller than in c-Si. This is caused by a considerable thermal desorption of Kr from a-Si at 580 K.[16] Also, the gas sputtering cross section σ_0 is a factor of 3 lower than derived for c-Si. This is probably related to the fact that in a-Si self-interstitial atoms are less effective in kicking out inert gas atoms from substitutional positions than in c-Si.[16] The inert gas escape depth λ_g is comparable with determinations from thermal-desorption spectrometry experiments. The sputtering yield Y_{Si} is, as expected, close to 0 for 50 eV Kr on Si.[22] The projected range R_p is larger than that found from a TRIM calculation. The fact that the growing film is held at a temperature of 580 K may have contributed to this. Probably Kr at a distance of 2–4 Å below the surface desorbs at this temperature. Kr in a-Si is immobile at this temperature, but in the near-surface situation some mobility is anticipated. Consequently, gas release at this temperature is expected from this zone. In addition, the fact that a fraction of about 5% of the Kr ions is doubly charged and consequently is implanted with double energy will result in a different depth profile.

TABLE II. Fitted parameters in Eq. (2) for a-Si, (1) TRIM and (2) experimental results (see Ref. 16) for c-Si.

	Y_{Si}	R_p(Å)	ΔR_p(Å)	η	λ_g (Å)	σ_0 (10^{-15} cm^2)
a-Si	0.0	15.9	3.7	0.035	5.9	1.34
c-Si	0.0[(1)]	9.25[(1)]	2.0[(1)]	0.30[(2)]	5[(2)]	4.0[(2)]

To investigate the variation of the Kr concentration as a function of depth perpendicular to the surface, we used energy dispersive spectrometry (EDS) on cross-sectional samples. The results of the KrSi sample with the highest Kr concentration, 5.8 at. %, is shown in Fig. 5. The Kr concentration rises steeply at the layer–bulk interface at 5.7 μm to a constant Kr concentration layer at 1 μm from the interface. These results were previously interpreted[10,18] as crystalline film growth with a low Kr concentration in the beginning of the deposition process, followed by amorphous growth with a much higher Kr concentration after some critical thickness. However, this artifact can be ascribed to an apparent shift of the interface due to a tilting of the sample during the EDS measurement. High-resolution electron microscopy analysis of these films (see Sec. V B) have indicated that there is indeed no sign of (poly)crystalline growth and that the Kr concentration is already high at the interface. The Kr concentration being constant over the deposited layer is corroborated by RBS experiments which monitor only the top 0.5 μm.

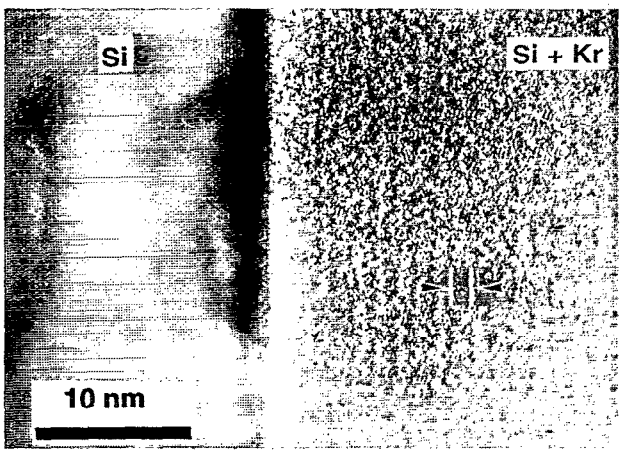

FIG. 6. High-resolution image of the Si substrate (left) in the ⟨110⟩ orientation, together with the amorphous layer of Kr*Si* (right). In the amorphous layer one can see sublayers (arrowed) with alternating dark and bright contrast, having a period of 1.3(1) nm.

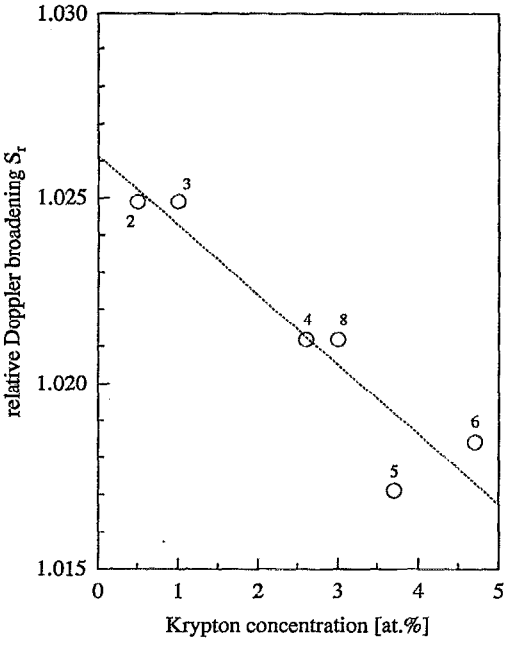

FIG. 7. Positron annihilation S parameter normalized to c-Si vs Kr concentration; see Table I.

B. High-resolution electron microscopy

For the HREM experiments a layer of 4.9 μm was deposited with $J_{Si}=3.4\times10^{15}$ and $J_{Kr}=1.3\times10^{16}$ cm^2 s^{-1} and a duty cycle of 30% at 0.5 Hz, resulting in an average Kr concentration of 4.8 at. %. The sample was prepared for cross-sectional HREM by cleaving the wafer into $2\times1\times0.5$ mm^3 chips, which were glued together with the thin layers facing each other. Next, the sample was dimpled to a thickness of 10 μm and ion-beam thinned to electron transparency. HREM observations were done using a JEOL 4000 EX/II electron microscope operated at 400 kV. This microscope has a point to point resolution of 0.13 nm.

Figure 6 shows a HREM micrograph of the substrate viewed in the ⟨110⟩ orientation together with the thin film. The film/substrate interface is sharp: there is no sign of polycrystalline growth in the region close to the substrate. Instead of clusters or bubbles of Kr atoms, a regular sequence of dark and bright bands is observed in the amorphous layer. These bands are interpreted as sublayers with alternating high and low average electron-scattering power. If an image is made with a small objective aperture, regions in which electrons are scattered at higher angles show up darker than the surrounding parts. It is indeed observed that the difference in contrast between the dark and bright band decreases with increasing objective aperture. Since Kr has a higher electron-scattering factor than Si, the dark and bright bands may be interpreted as layers with alternating high and low Kr concentration. The period of these sublayers is measured as 1.3(1) nm.

The formation of sublayers can be understood as resulting from the processing of the material: Si is continuously deposited at a rate of 0.65(10) nm s^{-1}, while Kr is injected with a duty cycle of 30% at 0.5 Hz. This indeed leads to a period of about 1.3 nm. Inert gas desorption experiments on Ar and Kr in a-Si did not detect any thermal mobility at all at temperatures below the crystallization temperature (~800 K).[23] Some irradiation induced mobility due to the inert gas bombardment may have occurred which might have led to an extra spread of at most 0.6 nm on top of the straggling of 0.4 nm expected for 50 eV Kr implantation. This small mobility explains why the Kr concentration has not been smeared out.

The maximum size of the agglomerates can also be inferred from HREM. The contrast will vanish if the average size of the agglomerates is larger than about 1 nm.

C. Positron beam analysis

Figure 7 shows values of the S parameter relative to c-Si, S_r, for the various samples versus the Kr concentration (open circles). The dotted curve serves to guide the eye. Basically the observation of a high S_r value indicates the presence of open volume defects. A value of $S_r=1.14$ was found for molecular-beam deposited (MBE) a-Si films at 250 °C, which indicates large microcavities.[16] Small vacancy-type defects lead to $S_r=1.02$. The value found for low Kr concentrations, $S_r=1.024$, is very close to that found for ion implanted a-Si relaxed at 773 K.[15] The present results clearly indicate that ion assisted growth leads to a strong reduction of open volume defects and points to the presence of small vacancy clusters. Interestingly, the cluster size seems to decrease with increasing Kr concentration. On the other hand, the positron diffusion length decreases from 14 nm at low Kr concentration to ≈7 nm for concentrations ≥3 at. % (see Fig. 8), indicating an increase of the number of trapping centers, presumably correlated with the incorporated Kr.

D. Raman spectroscopy

Raman spectroscopy is sensitive to structural changes because it detects changes in the vibrational frequencies due to local strain (bond bending).[17] Several studies indicate that there is a fundamental relation between the half-width at half

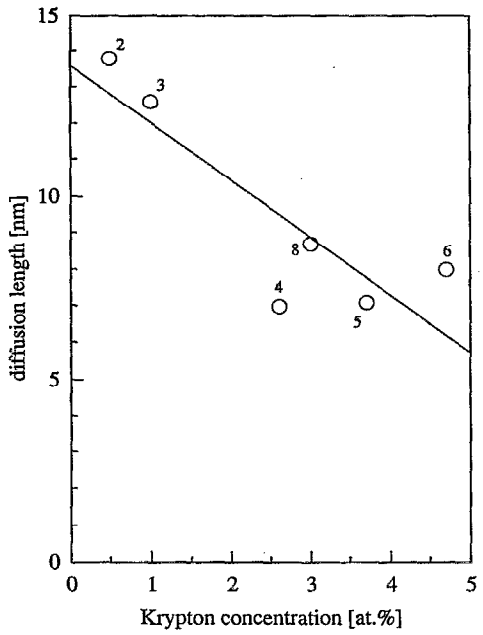

FIG. 8. Positron diffusion length vs Kr concentration; see Table I.

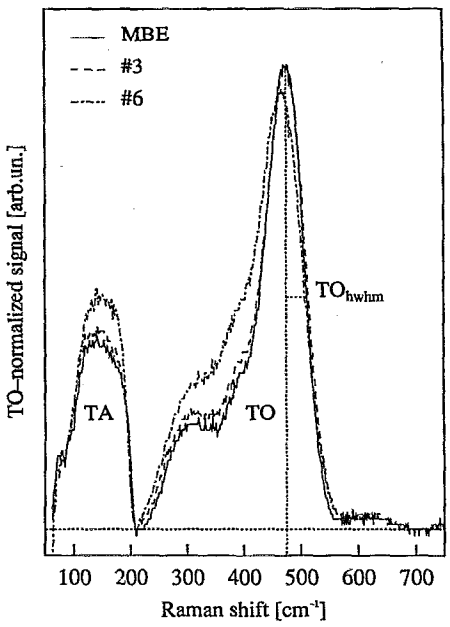

FIG. 9. Raman spectra of sputtered Kr*Si* layers for the indicated Kr concentrations, compared with MBE-grown *a*-Si; see Table I. The transverse optic (TO) and acoustic (TA) peaks are indicated. The half-width at half maximum of the transverse optic peak (TO_{hwhm}) is defined as indicated.

maximum of the main (transverse optic) peak in the Raman spectrum, TO_{hwhm}, and the average bond-angle distortion $\Delta\Theta$ in the amorphous Si network. However, there is no agreement between the quantitative relations between TO_{hwhm} and $\Delta\Theta$.[24] Beeman *et al.* (Ref. 17) derive for the relation between TO_{hwhm} and $\Delta\Theta$

$$2TO_{hwhm} \approx 15 + 6\Delta\Theta, \tag{5}$$

where TO_{hwhm} is given in cm^{-1} and $\Delta\Theta$ in degrees. Tsu *et al.* (Ref. 25) find, using a different approach

$$(2TO_{hwhm})^2 \approx (32)^2 + (6.75\Delta\Theta)^2. \tag{6}$$

Values of TO_{hwhm} obtained in different experiments range from 32 to 49 cm^{-1}, corresponding to values of $\Delta\Theta$ of 8.2°–13.8°. Over the experimentally accessible range $32 \leqslant TO_{hwhm} \leqslant 49$ cm^{-1} we note that Eqs. (5) and (6) are essentially indistinguishable. For an overview of Raman spectroscopy in relation with amorphous Si, we refer to Ref. 24.

The measurements were performed with the 514.5 nm line of an Ar-ion laser. The probe depth at this energy is approximately 0.1 μm for *a*-Si. Spectra were taken in quasi-backscattering geometry, using a triple-grating monochromator to disperse the scattered light onto a CCD detector. The spectra were fitted with a set of Gaussians. In order to avoid complications arising from the asymmetry of the spectrum, we determined the half-width at half maximum of the TO peak at the high-energy side of the peak.

In Fig. 9 we compare Raman spectra of *a*-Si prepared by molecular-beam epitaxy at 350 °C and two *a*-Si samples prepared by sputtering at 310 °C. The Kr concentration in the sputtered samples is 1 at. % for sample 3 and 4.7 at. % for sample 6 (see Table I). The Raman spectra of sample 3 and the MBE-deposited sample are nearly identical. The TO peak width of sample 6 is larger than that of the other two *a*-Si samples. This suggests that the disorder in the *a*-Si network increases with increasing Kr concentration. This is illustrated in Fig. 10 where we have plotted TO_{hwhm} as a function of the Kr concentration. The dotted lines are only to guide the eye. A value of 37.2(3) cm^{-1} was measured for an *a*-Si sample made by self-ion implantation and annealing at 583 K, in agreement with literature.[26] Additional annealing of the samples at 753 K leads to an overall decrease of the curve by $\approx$1.5 cm^{-1}. This suggests again that the structures of *a*-Si made by ion assisted deposition and by ion implantation with the lowest inert gas concentrations are very similar when compared at the same temperature. The increase in bond-angle distortion as a function of the Kr concentration is at least partly due to the strain introduced in the network by the relatively large Kr atoms. The observed variation in the bond-angle distortion as a function of the Kr concentration cannot be due to Kr agglomerates of appreciable size and thus points to the presence of isolated Kr or very small clusters, in corroboration with the PA results. The value found for Kr concentrations >3 at. % is very close to the value of 43 cm^{-1} found for *a*-Si self-ion implanted at low temperature.[26]

E. Mössbauer spectroscopy

Mössbauer spectra of Kr incorporated in Si have been measured. Because of the low energy of the Mössbauer line, the total Si thickness should not exceed about 50 μm. In order to get a reasonable effect, a thickness of >5 μm Si containing about 5 at. % ^{83}Kr is required. Therefore Kr enriched to 70% in ^{83}Kr was used for the preparation of the Mössbauer samples. However, it turned out to be very diffi-

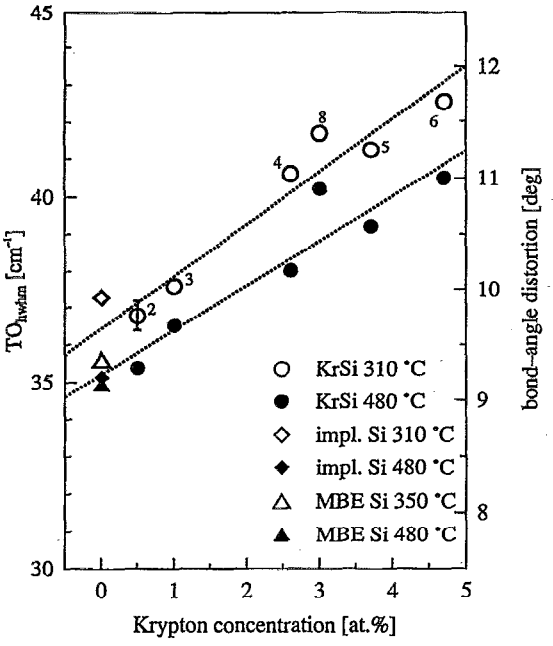

FIG. 10. Half-width of Raman peak TO_{hwhm} (left) and bond-angle distortion $\Delta\theta$ (right) vs Kr concentration; see Table I. Shown are the results for layers sputtered at 310 °C (open circles) and after subsequent annealing at 480 °C (closed circles). The error bar is indicated. In addition, measurements on self-ion implanted a-Si made at 77 K and after subsequent annealing at 310 (open diamonds) and 480 °C (closed diamonds) are shown, together with measurements on a-Si grown by molecular-beam epitaxy at 350 °C (open triangles) and after annealing at 480 °C (closed triangles).

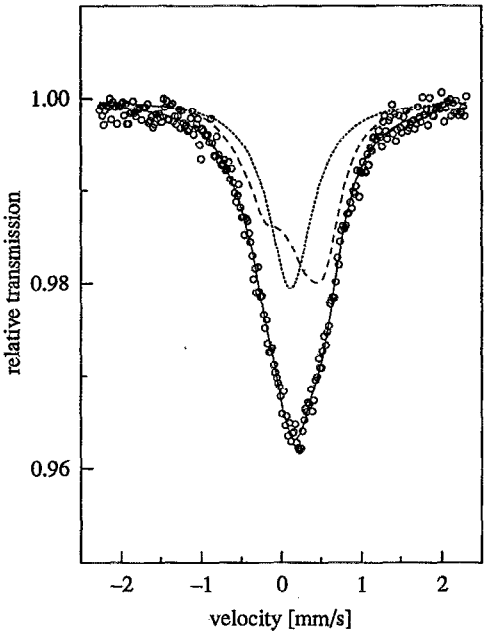

FIG. 11. ^{83}Kr Mössbauer spectrum taken at 4.2 K on a sputtered layer of 6 at. % Kr in Si on an Al backing. Source: ^{83}RbI at 4.2 K. The quadrupole-split nature of the source was taken into account. The parameters of the single line (solid) and quadrupole component (dotted) are listed in Table III.

cult to obtain a 10 μm thick ^{83}KrSi layer on a 25 μm Si⟨100⟩ wafer because of the stress induced in the thin substrate by the sputtered layer. Therefore we sputtered a 20 μm ^{83}KrSi layer on a 15 μm Al foil. Substrate bias and temperature were equal to the values mentioned above. A Kr concentration of 6 at. % was achieved by 0.5 Hz pulsation of the substrate at 50 V at a duty cycle of 10%. We used a ^{83}RbI Mössbauer source, dehydrated at 100 °C for half an hour under H_2 flow. The source spectrum consisted of a dominant narrow single line and an additional quadrupole component so that for the analysis account must be taken of the quadrupole-split nature of the source, as has been described in Ref. 11.

The Mössbauer spectrum obtained at 4.2 K on the as-deposited sample is shown in Fig. 11. It is tentatively fitted with a single line and a quadrupole component, both with isomer shifts much larger than found in the case of small Kr bubbles in Al.[11] It turned out to be impossible to include a line associated with solid Kr with an intensity larger than 1%. The fitted parameters are given in Table III. Spectra were taken as a function of absorber temperature between 4.2 and 200 K, while the source was kept at 4.2 K. Although the total absorber area showed fluctuations in the order of 10% due to different peak background ratios, no change in the total absorbed area was observed within the error bars. This indicates a lower limit for the characteristic Debye temperature of ≈250 K, i.e., a factor of 4 larger than the Debye temperature of solid Kr at 1 bar. Both the isomer shifts and the Debye temperature indicate that the Kr resides in very small clusters, consistent with the PA, Raman, and HREM results. A tentative explanation of these results is that the single line belongs to individual Kr atoms fourfold coordinated with Si atoms, while the quadrupole component is associated with Kr dimers, trimers, etc. in the amorphous Si matrix. The fraction of Kr bubbles is negligible. After annealing at 773 K, where relaxation of the a-Si is expected, no change in the measured spectrum was observed. Unfortunately, Mössbauer spectra cannot be obtained at higher annealing temperatures, because of the relatively low melting temperature of Al.

F. Bending and hardness measurements

For the bending experiments a layer of 21.2 μm was deposited on a 20 mm round, 250 μm thick Si⟨100⟩ wafer, with $J_{Si}=5.9\times10^{15}$ and $J_{Kr}=2.5\times10^{16}$ cm^2 s^{-1} and a duty cycle of 50% at 0.5 Hz, resulting in a local Kr concentration of 5.0 at. %. The sample shows a maximum bending of 160 μm at the center; see Fig. 12. This corresponds to a curvature radius $R=253$ mm. The stress in the film was calculated from the well-known Stoney equation[27,28] relating the substrate bending to a biaxial in-plane stress:

TABLE III. Parameters of Mössbauer spectrum of ^{83}KrSi at 4.2 K in mm s^{-1}.

S_S	S_Q	Δ	Γ_s	Γ_Q	A_S/A_Q
0.129(6)	0.244(6)	−1.78(2)	0.63(1)	0.48(1)	0.57(1)

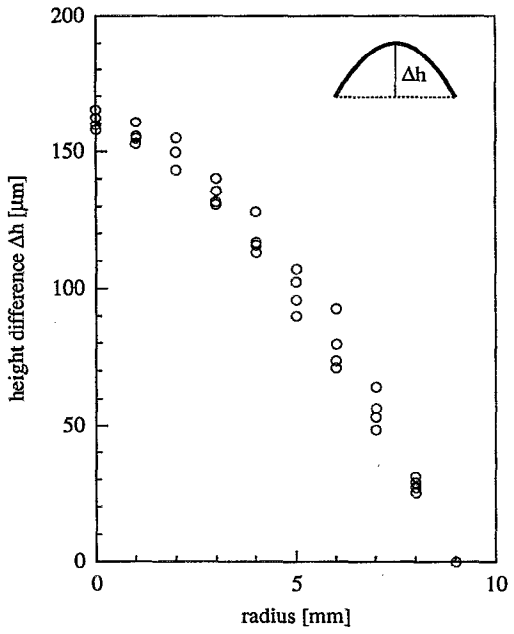

FIG. 12. Bending of a 21.2 μm thick Si layer sputtered on a 250 μm thick Si ⟨100⟩ wafer. The layer contains 5 at. % Kr.

$$\sigma=\frac{E_s}{1-\nu}\frac{t_s^2}{6Rt_f}, \tag{7}$$

where E_s and ν are the Young's modulus and Poisson ratio of the Si substrate, respectively, t the thickness, R the effective substrate radius of curvature, and the subscripts s and f refer to substrate and film, respectively. It is assumed that a plane-strain situation exists and that the bending can be described as a linear elastic event without plastic deformations of the substrate. Further, all other elements in the stress tensor are assumed to be zero, including a possible shear stress at the substrate/film interface and a stress normal to the plane of the substrate/film. Although near the edge of the film a substantial change of the stress state might occur and localized normal and shear stresses are important for adhesion, these components of the stress tensor are neglected. In Table IV the elastic constants of c-Si and polycrystalline pc-Si are listed. The Poisson ratio is given in terms of the Lamé constants λ and μ by[29]

$$\nu=\frac{\lambda}{2(\mu+\lambda)} \tag{8}$$

and the Young's modulus by

$$E=2\mu(1+\nu). \tag{9}$$

TABLE IV. Elastic constants of crystalline (c) and polycrystalline (pc) Si (see Ref. 29).

Si	μ (GPa)	λ(GPa)	E (GPa)	ν
c	79.6	63.7	165.2	0.223
pc	68.1	52.4	165.8	0.217

Under the given assumptions Eq. (7) yields a planar biaxial stress $\sigma_{xx}=\sigma_{yy}=\sigma=0.34$ GPa.

It has to be emphasized that Eq. (7) is only correct if $t_f \ll t_s$ and the elastic constants of the substrate are equal to those of the film. It has been pointed out[30,31] that Eq. (7) has to be modified to

$$\sigma=\frac{E_s}{1-\nu}\frac{t_s^2}{6Rf_t}\left[1-\frac{t_f}{t_s}\left(1-4\frac{E_f}{E_s}\right)\right] \tag{10}$$

upon relaxing the thickness and modulus restrictions. However, in the present case the stress calculated by the original Stoney equation turns out to be only 7% too high.

Wolfer[32] has derived an expression for the stress in a film containing a high concentration of pressurized bubbles. In our case the Kr atoms are probably distributed in the form of individual atoms or small clusters. However, this is not a serious problem, because Wolfer's expression remains correct if the word "bubble" is interpreted as an inclusion producing a local stress field at its surroundings. The stress field produced by such a "bubble" is, apart from a shear tensor, given by a hydrostatic stress σ_H, which for $R \leqslant r \leqslant r_c$ is given by

$$\sigma_H=\frac{\bar{p}S}{1-S}+\frac{(p-\bar{p})\alpha S}{1-\alpha S}, \tag{11}$$

where p is the pressure inside a bubble of radius R, $\bar{p}$ the average pressure of the bubbles in the material, S the volume fraction of the bubbles, r the distance from the bubble center, $r_c=R/S^{1/3}$ the linear size of the volume containing on the average one bubble, and α a function of shear and bulk modulus. Noordhuis *et al.*[33] used these expressions for their analysis of the nucleation of martensite in Ne implanted SS304. An important factor in the relation between the bubble pressure and the film stress forms the volume fraction S of the bubbles, which in our case, using a molar volume of 20 $cm^3\,mol^{-1}$ for Kr at pressures of the order of gigapascals,[34] amounts approximately to $S=8\%$. In the case of biaxial in-plane stress, we can write $\sigma_{zz}=0$ and $\sigma_{xx}=\sigma_{yy}=\sigma$ and consequently

$$\sigma_H=\tfrac{1}{3}(\sigma_{xx}+\sigma_{yy}+\sigma_{zz})=\tfrac{2}{3}\sigma. \tag{12}$$

Following the expressions given by Wolfer and taking $\bar{p}=p$, we find that an average hydrostatic pressure $\bar{p}=2.6$ GPa is necessary to produce a hydrostatic stress σ_H equal to 0.34 GPa. This pressure is very high and is usually only observed for inert gases in high melting temperature materials.[4]

If is of interest to see whether the high hydrostatic pressure can be related to the maximum stress the solid can take before fracture will occur. Therefore microhardness measurements were carried out, resulting in a Vickers hardness value of 1159 kgr mm^{-2}. This corresponds to a yield stress of the a-Si films of $\sigma_Y^a=3.86$ GPa and may be written in terms of the shear modulus $\mu^c=c_{44}$ of c-Si as $\sigma_Y^a=0.048\ \mu_c$. This value is in agreement with the following consideration. Regard an amorphous material as consisting of an irregular disclination network.[35,36] In contrast to a dislocation network the elastic energy stored in a disclination network would increase with the distance from a particular disclination, lead-

ing to a positive or negative curvature of the material. In order to compensate for this, assume that the network consists of positive and negative disclinations with a density ρ and a certain average distance $l=1/\sqrt{\rho}$ apart. Since radial distribution functions of amorphous materials in real space usually extend up the first-nearest neighbors with a certain correlation, the separation between the two disclinations in our supposed network is about $5b$, where b represents the magnitude of the Burgers vector. This implies a high disclination density of about 3×10^{17} m^{-2}. The yield stress of an amorphous material is now described as cutting of the disclination network by dislocations, i.e., it is related to opposing the line tension T as in the crystalline case: $\sigma_Y^a=2T(bl)$, where $T=\mu^c b^2\ln(l/b)/4\pi$ (see Ref. 29, p. 64). Assuming $l=5b$, we find $\sigma_Y^a=0.051\ \mu^c$, i.e., about 1/20 of the shear modulus of c-Si. Indeed this is close to the experimentally determined value. This simple model ignores any self-energy of dislocations as well as splitting of dislocations. Further, b is taken to be constant although the physical picture in fact suggests fluctuations of b due to the disclinations.

The question is whether we can make an estimate of the shear modulus μ^a of a-Si. A first-order approximation is to equate the theoretical yield stress and shear modulus of c-Si, $\sigma_Y^c=\mu^c$. Adopting this also for amorphous material, we can write $\sigma_Y^a=\mu^a=1/20\ \mu^c$. However, this is a lower bound value. Description of the local stress-displacement profile corresponding to an ideal fracture event by Frenkel (Ref. 37; see also Ref. 29, p. 6),

$$\sigma=\frac{\lambda c_{11}}{2\pi a}\sin\frac{2\pi x}{\lambda}, \tag{13}$$

predicts, when applied to a-Si, a maximum theoretical stress $\sigma_Y^a\approx0.4\ \mu^a$, where λ is the interatomic distance, a the planar spacing, and x the shear transition. Taking $\lambda\approx a$, this yields $\mu^a\approx0.1\ \mu^c$. At any rate, the fracture stress will be greatly reduced by the lower elastic moduli in the amorphous case. In this sense it is quite instrumental to look at the Griffith fracture stress σ_F for brittle materials at which spontaneous fracture will occur when the magnitude of the crack-extension and crack-resistant forces are equal:[38]

$$\sigma_F\approx\left(\frac{4\gamma E}{\pi d}\right)^{1/2}, \tag{14}$$

where γ is the surface energy per unit area and d represents the diameter of the crack. Taking the fracture stress equal to the earlier found pressure in the "bubble," $\sigma_F=\bar{p}=2.6$ GPa, $\gamma=1.2$ J m^{-2}, and the proposed reduction of the elastic constants, the largest stable crack diameter, i.e., size of the Kr inclusions, is, by using Eq. (14), ranging between 1.9 and 3.7 nm. In this analysis it is assumed that no extensive plastic deformation occurs upon crack propagation and that the surface free energy of a-Si is identical to the surface free energy of c-Si. We conclude that the Griffith criterion leads to values for the size of the Kr inclusions which are still too large compared with other estimates. This is not surprising in view of the fact that this criterion is based on a continuum description, and is consequently difficult to apply to inclusions of atomic size.

VI. SIMULATIONS

The question is whether the a-Si network is sufficiently rigid to account for a lower limit for the Debye temperature of the trapped Kr of 250 K as was measured with Mössbauer spectroscopy. We can use the following relation to estimate the Debye temperature of isolated Kr in Si:[11]

$$\Theta=\Theta_0 e^{\gamma_0(1-V/V_0)}, \tag{15}$$

where Θ is the Debye temperature, V the volume, γ the Grüneisen parameter, and the subscript 0 refers to the values at some reference temperature and pressure. Assuming that the volume available for an isolated Kr atom is equal to the atomic volume of Si, $V_0=12.05$ cm^3 mol^{-1}, and using the following values for Kr at the melting point at ambient pressure: $V=29.88$ cm^3 mol^{-1}, $\Theta_0=51.6$ K, and $\gamma_0=2.27$, we derive, for the Debye temperature of substitutional Kr in unrelaxed Si, $\Theta=200$ K. Although this approach might not be valid for these large volume differences, it illustrates that the experimental lower limit is surprisingly large. If the Si lattice is allowed to relax around the incorporated Kr atom, the volume the Kr occupies will increase and the Debye temperature according to Eq. (15) will decrease.

In order to understand the nature of the extremely large Debye temperature as derived from the Mössbauer experiments, molecular-dynamics simulations of Kr in a-Si were performed. The Si–Si interaction is described by the Stillinger–Weber potential,[39] the Kr–Kr interaction by the $K2$ potential of Barker.[40] A Kr–Si interaction potential has been constructed on basis of the model by Wilson and Bisson.[41] In this method the total energy of the interaction between two spherical charge distributions is calculated by the contribution of the electron–electron, electron–nucleus, and nucleus–nucleus electrostatic interactions and an additional exchange energy. This approximation results in a repulsive interaction potential. The data can be represented by a pair potential of the form

$$V(R)=V_0 e^{-R/\delta}, \tag{16}$$

where $V_0=2981$ eV, $\delta=0.288$ Å, and R is the interatomic distance. A similar form of the interaction potential for the inert gas–metal system has been proposed by Jensen *et al.*[42] and Fearn *et al.*[43] based on an embedded-atom approach.

Initially, 216 Si atoms are arranged on a diamond lattice with $3\times3\times3$ unit cells, using periodic boundary conditions. The Kr atoms are placed on substitutional Si lattice sites. Simulations were performed at constant volume with the lattice constant of Si at room temperature, 5.43072 Å. The leap-frog integration scheme was used for solving Newton's equation of motion. The system is coupled to a temperature bath by the coupling constant τ, as has been described by Berendsen *et al.*[44] In order to simulate the amorphous structure, the system is heated from room temperature for a few femtoseconds to a temperature of 30 000 K and subsequently allowed to relax to a temperature in the range from 300 to 1500 K with the temperature bath coupling constant arbitrary set to $\tau=10$ fs. The amorphous structure obtained in this way is compared with experimental data on the radial distribution function and the distribution of bond angles. In Fig. 13 the relaxation of the heated system as a function of the heating

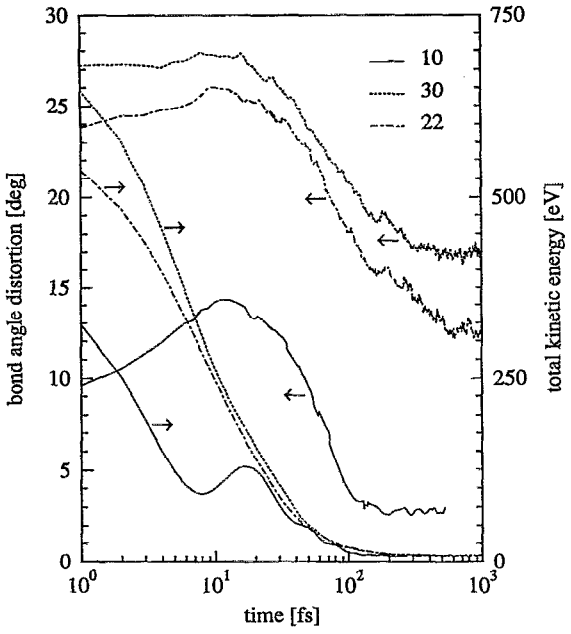

FIG. 13. Variation of bond-angle distortion (left) on temperature of computer modeled amorphous Si. The systems are heated for the indicated times at 30 000 K and are cooled down to 293 K. The corresponding total kinetic energy of the system is indicated at the right-hand scale.

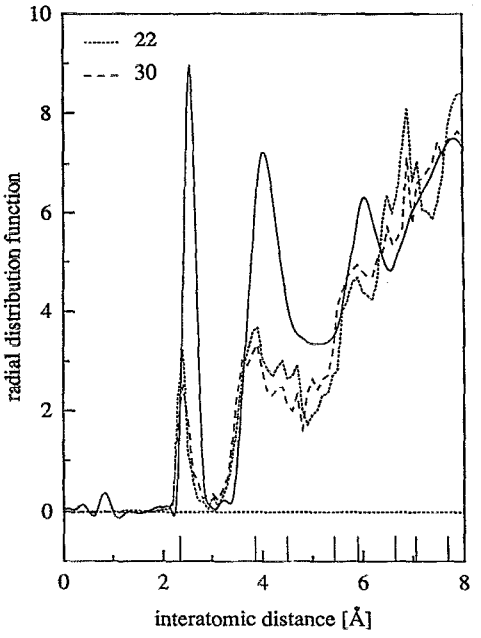

FIG. 14. Radial distribution function of computer modeled amorphous Si. The solid line represents experimental data (see Refs. 46 and 47), whereas the dotted curves represents data of amorphous Si heated for 22 and 30 fs at 30 000 K.

time is shown. The system which has been heated for 22 fs from room temperature up to 30 000 K shows upon quenching a relaxation of the bond-angle distortion from 23.8° to 12.6(3)°, whereas the systems heated for 10 and 30 fs exhibit a final bond-angle distortion of 2.8(1)° and 16.9(2)°, respectively. If the system has not been taken too far away from the initial c-Si structure, it will find its way back to its initial configuration and reestablish the crystalline order. But after some critical time, we have created a "inextricably entangled skein," which cannot return to crystalline order by a sequence of simple local rearrangements.[45,46] In Fig. 14 the radial distribution functions (RDF) of the heated systems are compared with the experimental RDF of a-Si.[46,47] Whereas the system heated for 10 fs exhibits a more crystalline than amorphous nature, the 22 and 30 fs heated systems exhibited a reasonable resemblance with the experimental RDF. Because the mean bond-angle distortion of the structure heated for 22 fs compares well with the experimental value ($\approx 10°$), we decided to perform our simulations of Kr in a-Si with this structure. Because the modeling of the amorphous network is far from perfect, we consider our results to be only semiquantitative.

Kr is inserted in the a-Si network on a substitutional site, and subsequently the system is allowed to relax to its lowest energy configuration at the given volume and temperature. We check the stability of the a-Si network by monitoring the bond-angle distortion. At the lowest temperature, $T=293$ K, the bond-angle distortion is constant over the simulation time, 5000 fs. At $T=600$ K however, the bond-angle distortion starts to decrease, reflecting the relaxation of the amorphous network. At the highest temperatures, $T=1200$ and 1500 K, the decrease in bond-angle distortion after 5000 fs is approximately 4°. In Fig. 15 the amorphous Si network with one substitutional Kr atom is shown. After having established equilibrium, the position of the Kr atom is monitored, from which the root-mean-square amplitudes can be obtained. The recoilless fraction f follows from

$$f = e^{-k^2\langle x^2\rangle}, \tag{17}$$

where $\mathbf{k}$ is the wave vector of the Mössbauer radiation, emitted along the x axis. In Fig. 16 we have plotted the temperature dependence of the recoilless fraction of an isolated Kr in a-Si. Although the scattering of the data is quite large ($\Delta f \approx 0.1$), we have fitted the data with a Debye model. This

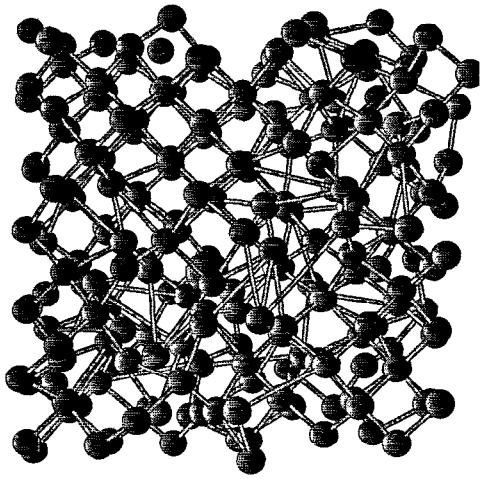

FIG. 15. Model of amorphous Si with one Kr monomer.

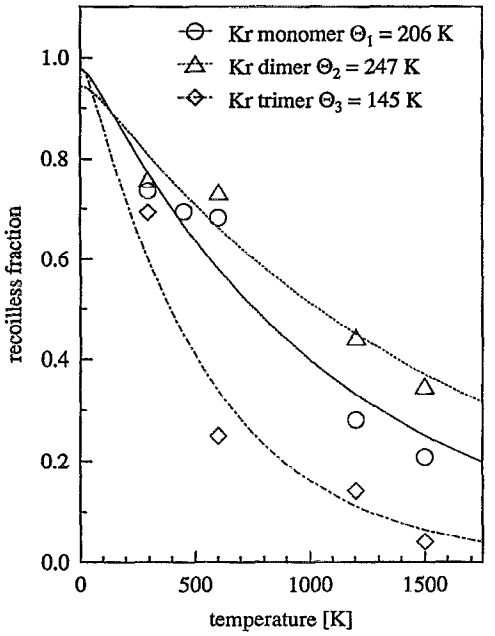

FIG. 16. Recoilless fraction vs temperature of a Kr mono-, di-, and trimer at substitutional sites in amorphous Si. The data is fitted to a Debye model, yielding the indicated Debye temperatures for the various agglomerates.

yields a Debye temperature Θ_1 of the Kr monomer of Θ_1=206(10) K. This corresponds surprisingly well to the estimated Θ=200 K based on Eq. (15). In addition, we performed simulations on Kr dimers and trimers in the amorphous Si network. The recoilless fraction data on the Kr dimers yielded an effective Debye temperature Θ_2=247(14) K, whereas the Kr trimers show a significant decrease in the Debye temperature, Θ_3=145(6) K. If we compare these results with the lower limit for the Debye temperature as measured with Mössbauer spectroscopy, Θ=250 K, we can conclude from the simulations that the Kr is present predominantly in mono- and dimers.

VII. THE EFFECT OF ALTERNATING Kr CONCENTRATIONS

The question arises whether the pulsed deposition technique for the production of the *a*-Si layers would affect our conclusions based on the deposition model, the positron annihilation and Raman measurements in which a continuous Kr deposition was assumed. As can be seen from the HREM picture in Fig. 6, the injection of Kr at a duty cycle of 30% at 0.5 Hz results in an alternating Kr concentration through the *a*-Si layer with a period of 1.3(1) nm. The layers deposited with a low-flux ratio and a duty cycle of 1%–5% were deposited with a pulsation frequency of 10 Hz. Consequently, in these layers the Kr implantation profile overlaps the Si deposition, so we do not expect to observe alternating Kr concentrations in these layers. Also, for the layers deposited with a high-flux ratio and a duty cycle larger than 50% at 0.5 Hz, no alternating Kr concentration is expected. However, in the intermediate-flux regime, corresponding to the Kr concentrations larger than 4 at. % with duty cycles of 10%–50% at 0.5 Hz, the discussion about average concentrations might not be maintained. However, in both the positron annihilation and the Raman experiment, Figs. 7 and 10, we observe no abnormal change in the behavior for the *S* parameter and the bond-angle distortion versus average Kr concentration. This is expected if there is a linear relationship between these quantities and the Kr concentration so that the average *S* parameter and bond-angle distortion nearly equals the value of these quantities for a uniform layer with the average Kr concentration. The fact that we indeed observe such a linear relationship supports this assumption. Therefore we do not expect that the pulsation of the Kr flux will change the main conclusions drawn. With regard to the effect on the parameters derived from the deposition model, an appropriate calculation should be performed.

VIII. DISCUSSION

The results obtained with the different techniques applied to the *a*-Kr*Si* system have led us to the following general picture of the incorporation of Kr. During all steps of the process of implantation at low energy while Si is sputter deposited, the Kr is not able to move over distances larger than 0.5 nm. This has followed from the HREM observation of a multilayer structure of alternating *a*-Si and *a*-Kr*Si* layers. This result is in line with the value of the attenuation length of 0.59 nm adopted in the gas incorporation model we used. Positron annihilation measurements show that there is a negligible open volume associated with the Kr, and Raman measurements indicate a considerable bond-angle distortion. The results together with the Mössbauer results point to the presence of mono- or dimer Kr inclusions in the deposited film. The finding of high stress corroborates these conclusions.

Roorda *et al.*[26] have shown that the defect formation and annihilation processes are similar in amorphous and heavily damaged crystalline Si. It is expected that the long-range mobility of point defects, e.g., self-interstitials and vacancies, in *a*-Si is strongly reduced by the presence of a high concentration of traps. Therefore the implantated Kr will remain surrounded by Frenkel pairs it created. Short-range recombination of the Frenkel pairs may take place spontaneously or by the continuing bombardment with other Kr ions. In low-energy ion bombardment with heavy ions, surface atoms are pushed inward, leaving vacancy sites at the surface.[48] Therefore one may consider the net effect as self-interstitial implantation. The excess self-interstitials introduced in a random covalent network will cause the density to increase and will thus approach the density of the ideal network. Self-interstitials near an incorporated Kr atom will be adsorbed by the excess volume present around the Kr.

This behavior in *a*-Kr*Si* is in contrast with inert gases in bulk *c*-Si. In *c*-Si it has been shown by thermal-desorption spectrometry that implanted inert gas is strongly bound to vacancies in Si[49] corresponding with dissociation temperatures of about 800 K for a single Ar and 1180 K for a pair of Ar atoms. On the other hand, self-interstitials have proven to be able to remove the vacancies by recombination. The interstitial inert gas then may move away and be released. Apparently the latter process is reduced in the case of *a*-Si.

This is supported by the observation that during crystallization of a-Si Kr does not remain in the crystallized parts.[49] It is pulsed out from c-Si toward the a-Si/c-Si interface. Thus there is a higher solubility for Kr in a-Si than in c-Si. In turn this explains why the Kr shows less tendency to cluster. For concentrations smaller than 10 at. % and a temperature of 580 K, we observed no sign of precipitation. Usually there is no nucleation barrier for inert gas precipitates in any material where the solubility is low. The Gibbs free energy of the system will decrease by growth of the clusters because of surface energy arguments. However, the driving force may be smaller in a-Si than in c-Si and, moreover, the very low mobility of the gas in a-Si will prohibit the cluster growth.

IX. CONCLUSION

Several techniques have been applied to reveal the properties of Kr incorporated in sputter-deposited a-Si.

Upon varying the sputtering parameters the maximum concentration of Kr was found for a Si to Kr flux ratio of 4 for 50 eV Kr ions. A model describing the Kr concentration in terms of implantation, surface sputtering, growth, thermal diffusivity, and gas sputtering is able to predict the data when a negligible thermal diffusivity and a radiation induced diffusivity of <1 nm is assumed. Positron annihilation measurements indicate a rather well densified material with strongly reduced open volume of the defects. In addition, Raman spectroscopy revealed a strong bond-angle distortion like in a-Si layers made by self-ion implantation. Mössbauer spectroscopy results indicated a Kr Debye temperature larger than 250 K. HREM observations on a multilayer structure with alternating Kr concentration gave direct evidence of the low mobility of the incorporated Kr. Measurement of the compressive stress showed that the Kr was under very high pressure. The results can be understood when it is assumed that Kr is incorporated as isolated atoms or in very small clusters.

ACKNOWLEDGMENTS

The authors are indebted to J. H. Evans, G. Boom, U. Nieborg, and J. de Roode for their contributions. This work was performed as a part of the research program of the Stichting voor Fundamenteel Onderzoek der Materie (FOM), with financial support from the Nederlandse Organisatie voor Wetenschappelijk Onderzoek (NWO).

[1] R. S. Barnes, Philos. Mag. **5**, 635 (1960).
[2] A. vom Felde, J. Fink, Th. Müller-Heinzerling, J. Pflüger, B. Scheerer, and G. Linker, Phys. Rev. Lett. **53**, 922 (1984).
[3] C. Templier, C. Jaouen, J.-P. Rivière, J. Delafond, and J. Grilhé, C. R. Acad. Sci. (Paris) **299**, 613 (1984).
[4] C. Templier, in *Fundamental Aspects of Inert Gases in Solids*, edited by S. E. Donnelly and J. H. Evans (Plenum, New York, 1991), p. 117.
[5] M. G. Norton, E. L. Fleischer, W. Hertl, C. B. Carter, J. W. Mayer, and E. Johnson, Phys. Rev. B **43**, 9291 (1991).
[6] C. W. Allen and R. C. Birtcher, Mater. Res. Soc. Symp. Proc. **74**, 351 (1987).
[7] C. Templier, B. Boubeker, H. Garem, E. L. Mathé, and J. C. Desoyer, Phys. Status Solidi A **92**, 511 (1985).
[8] J. C. Desoyer, C. Templier, J. Delafond, and H. Garem, Nucl. Instrum. Methods B **19/20**, 450 (1987).
[9] M. J. W. Greuter, G. L. Zhang, L. Niesen, F. J. M. Buters, and A. van Veen, in *Fundamental Aspects of Inert Gases in Solids*, edited by S. E. Donnelly and J. H. Evans (Plenum, New York, 1991), p. 231.
[10] M. J. W. Greuter, L. Niesen, and A. van Veen, Mater. Res. Soc. Symp. Proc. **279**, 363 (1992).
[11] M. J. W. Greuter and L. Niesen, J. Phys. Condens. Matter. **5**, 3541 (1993).
[12] A. van Veen, in *Erosion and Growth of Solids Stimulated by Atom and Ion Beams*, edited by G. Kiriakidis, G. Carter, and J. L. Whitton, NATO ASI Ser. E, Vol. 112 (Nijhoff, Dordrecht, 1986), p. 200.
[13] W. O. Hofer, in *Erosion and Growth of Solids Stimulated by Atom and Ion Beams*, edited by G. Kiriakidis, G. Carter, and J. L. Whitton, NATO ASI Ser. E, Vol. 112 (Nijhoff, Dordrecht, 1986), p. 1.
[14] K. R. Bijkerk, A. van Veen, G. J. van der Kolk, and T. Minemura, J. Less Common Met. **145**, 189 (1988).
[15] R. A. Hakvoort, S. Roorda, A. van Veen, M. J. van den Boogaard, F. J. M. Buters, and H. Schut, Mater. Sci. Forum **105–110**, 1391 (1992).
[16] A. van Veen, M. J. W. Greuter, L. Niesen, B. Nielsen, and K. G. Lynn, Mater. Res. Soc. Symp. Proc. **262**, 181 (1992).
[17] D. Beeman, R. Tsu, and M. F. Thorpe, Phys. Rev. B **32**, 874 (1985).
[18] M. J. W. Greuter, L. Niesen, R. A. Hakvoort, J. de Roode, A. van Veen, A. J. M. Berntsen, and W. G. Sloof, Hyperfine Interactions **79**, 669 (1993).
[19] E. V. Kornelsen, Can. J. Phys. **42** (1964).
[20] H. A. Filius and A. van Veen, Radiat. Eff. **108**, 1 (1989).
[21] G. F. Bastin, H. J. M. Heijligers, and F. J. J. van Loo, Scanning **8**, 45 (1986).
[22] W. Eckstein, in *Computer Simulation of Ion–Solid Interactions* (Springer, Berlin, 1991), p. 203.
[23] A. van Veen, C. C. Griffioen, and J. H. Evans, Mater. Res. Soc. Symp. Proc. **107**, 449 (1988).
[24] W. C. Sinke, S. Roorda, and F. W. Saris, J. Mater. Res. **3**, 1201 (1988).
[25] R. Tsu, J. Gonzalez-Hernandez, and F. H. Polak, Solid State Commun. **54**, 447 (1985).
[26] S. Roorda, W. C. Sinke, J. M. Poate, D. C. Jacobsen, S. Dierker, B. S. Dennis, D. J. Eaglesham, F. Spaepen, and P. Fuoss, Phys. Rev. B **44**, 3702 (1991).
[27] G. G. Stoney, Proc. R. Soc. London **82**, 172 (1909).
[28] T. Adler and C. R. Houska, J. Appl. Phys. **50**, 3288 (1979).
[29] J. P. Hirth and J. Lothe, in *Theory of Dislocations* (Wiley, New York, 1982), p. 42 and 837.
[30] A. Brenner and S. Senderoff, J. Res. NBS **42**, 105 (1942).
[31] D. E. Fahnline, C. B. Masters, and N. J. Salamon, J. Vac. Sci. Technol. A **9**, 2483 (1991).
[32] W. G. Wolfer, Philos. Mag. A **59**, 87 (1989).
[33] J. Noordhuis and J. Th. M. de Hosson, Acta Metall. Mat. **38**, 2067 (1990).
[34] A. Polian, J. M. Besson, M. Grimsditch, and W. A. Grosshans, Phys. Rev. B **39**, 1332 (1989).
[35] N. River, Philos. Mag. A **40**, 859 (1979).
[36] J. F. Sadoc and R. Mossezi, Philos. Mag. B **45**, 467 (1982).
[37] J. Frenkel, Z. Phys. **37**, 572 (1926).
[38] A. A. Griffith, Philos. Trans. R. Soc. London, Ser. A **221**, 163 (1920).
[39] F. H. Stillinger and T. A. Weber, Phys. Rev. B **31**, 5262 (1985).
[40] J. A. Barker, R. O. Watts, J. K. Lee, T. P. Schafer, and Y. T. Lee, J. Chem. Phys. **61**, 3081 (1974).
[41] W. D. Wilson and C. L. Bisson, Phys. Rev. B **3**, 3984 (1971).
[42] K. O. Jensen and R. M. Nieminen, Phys. Rev. B **36**, 8219 (1987).
[43] M. Fearn, K. O. Jensen, and A. B. Walker, J. Phys. Condens. Matter **4**, 5479 (1992).
[44] H. J. C. Berendsen, J. P. M. Postma, W. F. van Gunsteren, A. DiNola, and J. R. Haak, J. Chem. Phys. **81**, 3684 (1984).
[45] J. Tyndall, in *Heat—A Mode of Motion*, edited by Longmans (Green, London, 1863).
[46] D. Weaire and F. Wooten, in *Physics of Disordered Materials*, edited by D. Adler, H. Fritzsche, and S. R. Ovshinsky (Plenum, New York, 1985), p. 1.
[47] F. Wooten, K. Winer, and D. Weaire, Phys. Rev. Lett. **54**, 1392 (1985).
[48] N. Herbots, B. R. Appleton, T. S. Noggle, R. A. Zuhr, and S. J. Pennycook, Nucl. Instrum. Methods B **13**, 250 (1986).
[49] A. van Veen, P. C. de Jong, K. R. Bijkerk, H. A. Filius, and J. H. Evans, Mater. Res. Soc. Symp. Proc. **100**, 231 (1988).